

11 Material Modeling Case Studies

Chapter Outline

11.1 Introduction	455
11.2 Acrylate-Butadiene Rubber	455
11.3 Chloroprene Rubber	460
11.4 Nitrile Rubber	464
11.5 Santoprene	468
11.6 High-Density Polyethylene	474
11.7 Polytetrafluoroethylene	479
11.8 Polyethylene Terephthalate	487
11.9 Polyether Ether Ketone	490
11.10 Exercises	496
References	497

11.1 Introduction

The previous chapters covered different experimental testing techniques, a continuum mechanics review, and a variety of different material models. This chapter will combine these topics into concrete case studies illustrating how different material models work by comparing the accuracy of the different approaches. The goal is to present, by example, what works and what does not work. Each case study covers a different material, or material class, and all results presented here were obtained using MCalibration.

11.2 Acrylate-Butadiene Rubber

Acrylate-Butadiene rubber (ABR) is a synthetic saturated rubber that is used in sealing and packaging applications. The mechanical response of ABR is characteristic of most elastomers and

consists of non-linear viscoelasticity (non-LVE) with significant strain-rate dependence.

Figures 11.1 and 11.2 show uniaxial compressive data for a lightly filled ABR. The material was tested at two true strain rates of $-0.01/\text{s}$ and $-0.1/\text{s}$, using compression followed by unloading segments. The cyclic response of the material was also examined by compressing the material to a true strain of -0.3 , followed by 600 strain cycles with a strain amplitude of 2.5% at 1 Hz . The average stress in the material is shown to relax during the cyclic loading.

The experimentally determined mechanical response of the ABR can be represented using many different material models, some of which work better than others. Since ABR exhibits hysteresis and energy dissipation during cyclic loading one cannot expect a hyperelastic model to provide an accurate representation of the material response. Figure 11.3 shows the best possible calibration of the Yeoh hyperelastic model (see Section 5.3.8). This model has an average error (calculated using the NMAD error measured defined in Equation (9.5)) of 17% . As shown in Table 11.1, other hyperelastic models will have similar errors in the predictions.

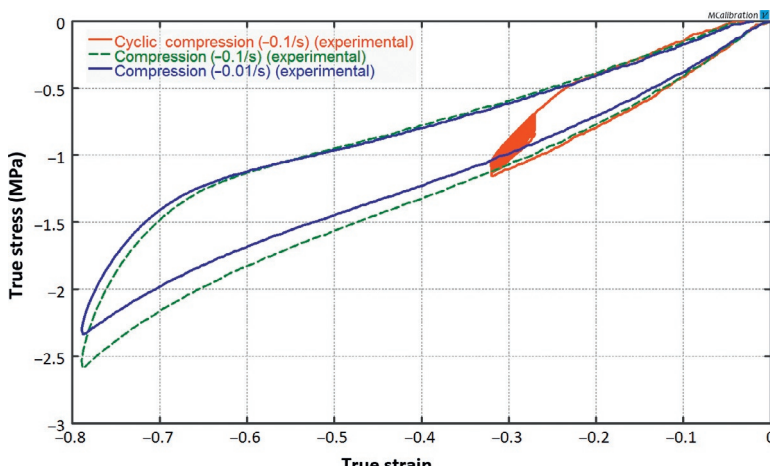


Figure 11.1 Uniaxial compression data for ABR at two different strain rates.

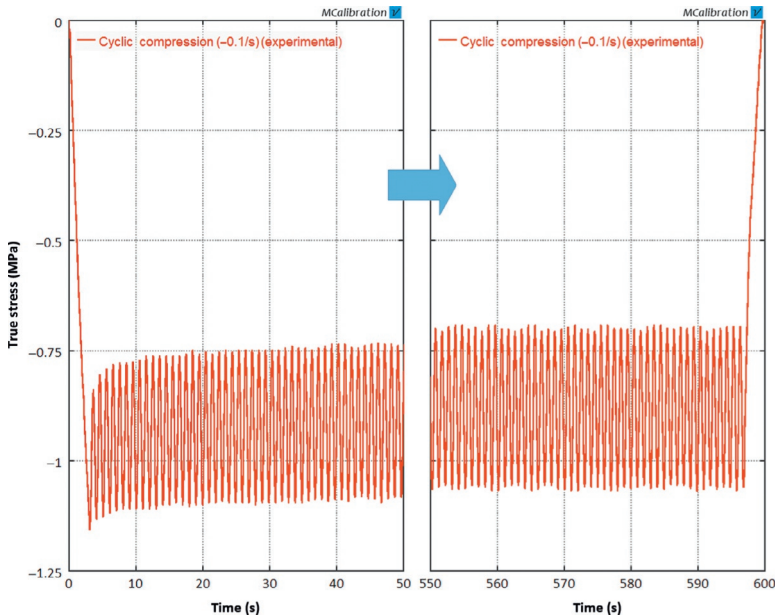


Figure 11.2 Stress-time response of the ABR during the first 50 and the last 50 load cycles.

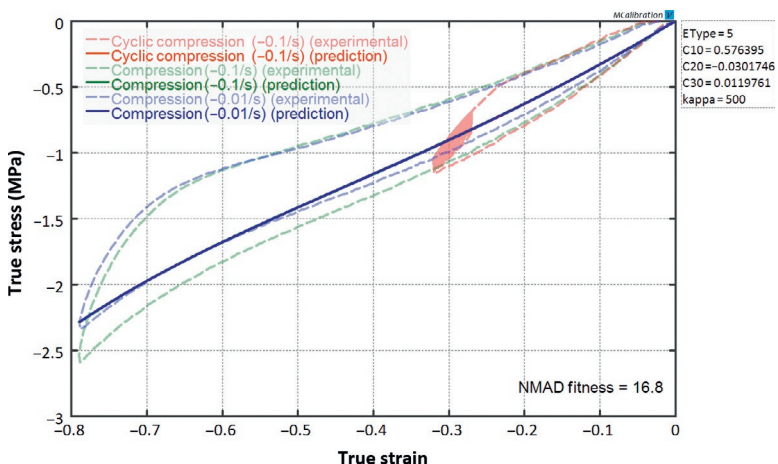


Figure 11.3 Comparison between experimental data for ABR and the best model predictions from the Yeoh hyperelastic model.

Table 11.1 Summary of Results from Material Model Calibrations for the ABR

Material Model	Error in Model Calibration (%)
Arruda-Boyce eight-chain	16.9
Yeoh	16.8
Linear viscoelasticity (Yeoh, five Prony series terms)	9.8
Three Network model	6.9
Bergstrom-Boyce (BB)	6.8
BB with Mullins damage	3.0
Higher order Parallel Network models with Mullins damage	3.0

Another candidate material model is LVE combined with Yeoh hyperelasticity (see Chapter 6). Since the strains in this case are relatively large it is no surprise that LVE does not accurately capture the material response. [Figure 11.4](#) compares the experimental data with the predictions from LVE (based on Yeoh hyperelasticity and five Prony series terms). The average error is about 10%, which is better than for hyperelasticity but still not an accurate representation of the true response.

To accurately represent the response of this material requires a nonlinear viscoelastic material model. [Figure 11.5](#) shows the predictions from the Bergstrom-Boyce (BB) model (see Section 8.2) with Ogden-Roxburgh Mullins damage (see Section 5.7.1). This model does an excellent job at capturing the material response. The average error in the predictions is about 3% (as determined by the NMAD fitness value). To achieve this level of accuracy it is necessary to include Mullins damage in the model in order to capture the increased tangent stiffness right after strain reversal. It would, of course, have been nice to have additional experimental

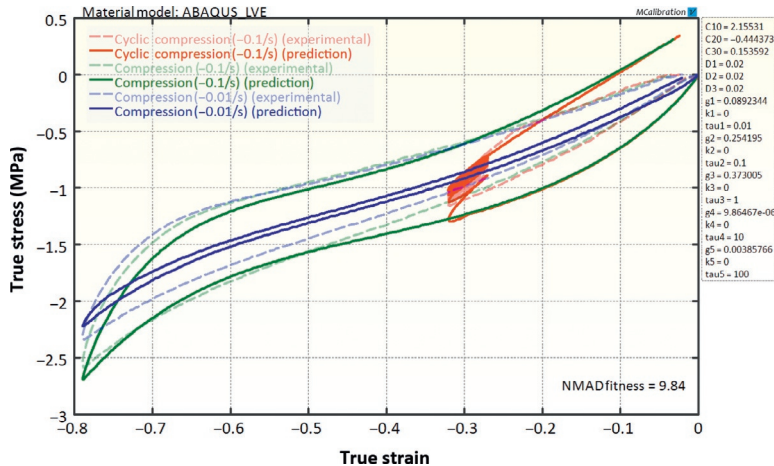


Figure 11.4 Comparison between experimental data for ABR and the best model predictions from a linear viscoelastic material model based on Yeoh hyperelasticity. The linear viscoelastic model was based on a five-term Prony series.

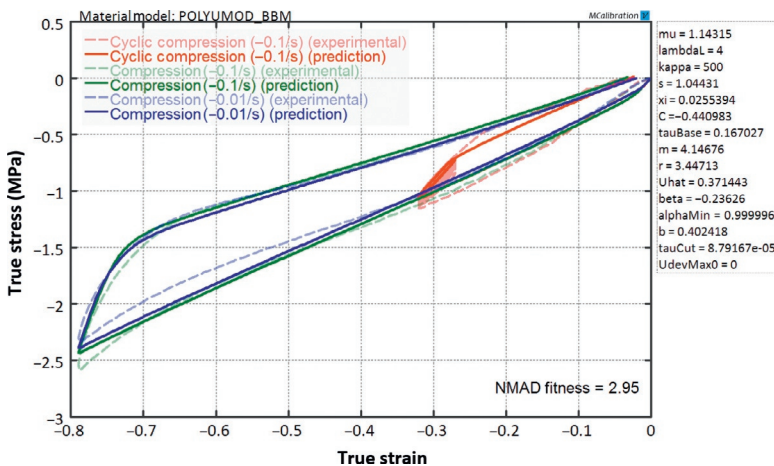


Figure 11.5 Comparison between experimental data for ABR and the best model predictions from BB model with Mullins softening.

data in order to further validate the accumulation of Mullins damage at different strain levels.

The original version of the BB model (without Mullins damage) in this case has an average error of 7%. The BB model is special case of the Parallel Network (PN) model that was covered

in Section 8.7 of Chapter 8 that is using two parallel networks. Adding additional network in this case does not provide any additional truthfulness to the predictions. As is often the case for rubbers, the Three Network (TN) model (see Section 8.6) is less accurate than the BB model even though it has three nonlinear viscoplastic networks compared to only two for the BB model. The reason for the superior predictions of the BB model is its Equation (8.19) for the viscoelastic flow rate that also considers the strain-dependence of the viscosity.

11.3 Chloroprene Rubber

Chloroprene rubber (CR) is a synthetic rubber that is also known by the trade name Neoprene. CR has a good balance of properties, including good chemical stability and usefulness over a wide temperature range. Examples of the uniaxial compressive response are summarized in Figures 11.6 and 11.7. The rubber material was tested at four different strain rates in uniaxial compression to a true strain of -0.8 , followed by unloading back to zero stress. Some of the experiments contained 30 s long stress relaxation segments during both the loading and the unloading.

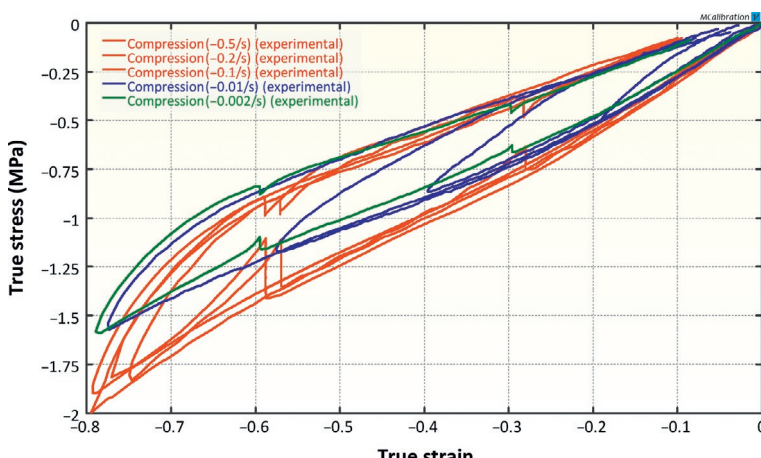


Figure 11.6 Uniaxial compression data for a CR with 7 vol% carbon black.

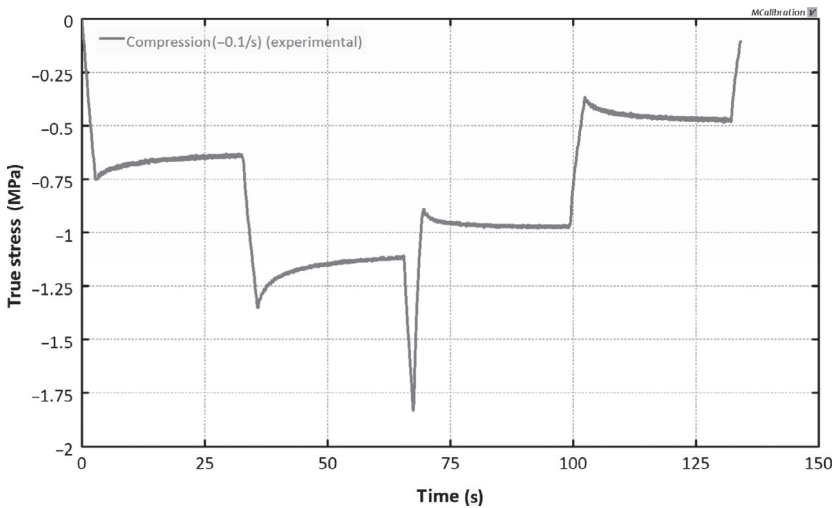


Figure 11.7 Stress relaxation response of a CR with 7 vol% carbon black.

Table 11.2 Summary of Results from Material Model Calibrations for the Chloroprene Rubber

Material Model	Error in Model Calibration (%)
Arruda-Boyce eight-chain	18.7
Yeoh	17.6
Linear viscoelasticity (Yeoh, five Prony series terms)	9.9
BB	5.6
BB with Mullins damage	4.4
Three Network model	6.0
Parallel Network model with BB-type flow and Mullins damage	4.2

Similar to the example in the previous section, CR can be represented using different material models. Table 11.2 summarizes the accuracy of various alternative material models. Like virtually all elastomers, CR exhibits hysteresis during cyclic loading, so a

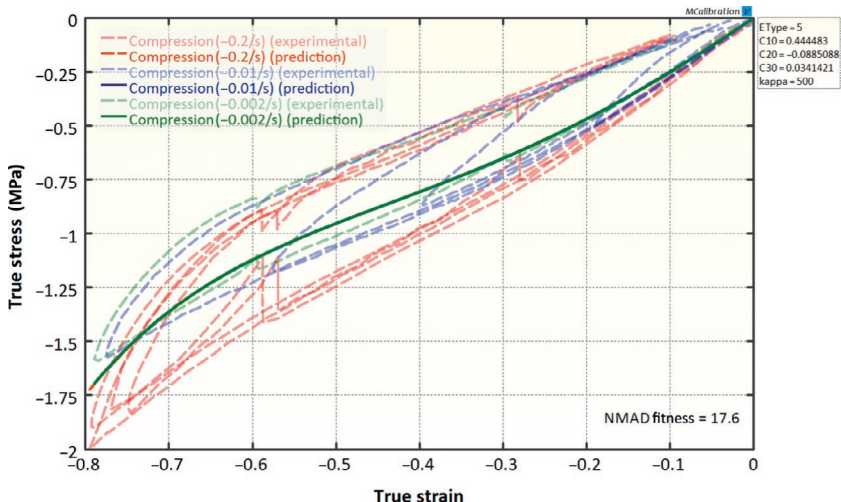


Figure 11.8 Comparison between experimental data for CR and the best model predictions from the Yeoh hyperelastic model.

hyperelastic model is unable to accurately represent the material behavior. As is shown in Figure 11.8, the best Yeoh hyperelastic model (see Section 5.3.8) has an average error of 18% (calculated using the NMAD error defined in Equation (9.5)). Other hyperelastic material models have similar predictive accuracy.

A slightly more advanced material model is LVE. Figure 11.9 shows the predicted stress-strain response of a Yeoh hyperelasticity-based linear viscoelastic model with five Prony series terms. The error of the stress-strain predictions is about 10%. This model does not provide accurate predictions of the material response, but is more accurate than a hyperelastic model.

An accurate material model for the CR is the BB model (Section 8.2) with Ogden-Roxburgh Mullins damage (Section 5.7.1). The average error in the model predictions is about 4.4%. Also in this case, this level of accuracy can only be obtained by combining non-LVE from the BB model with Mullins damage in order to capture the increased tangent stiffness right after strain reversal. If the BB model is used without Mullins damage then the error in the model predictions is about 6% (Figure 11.10).

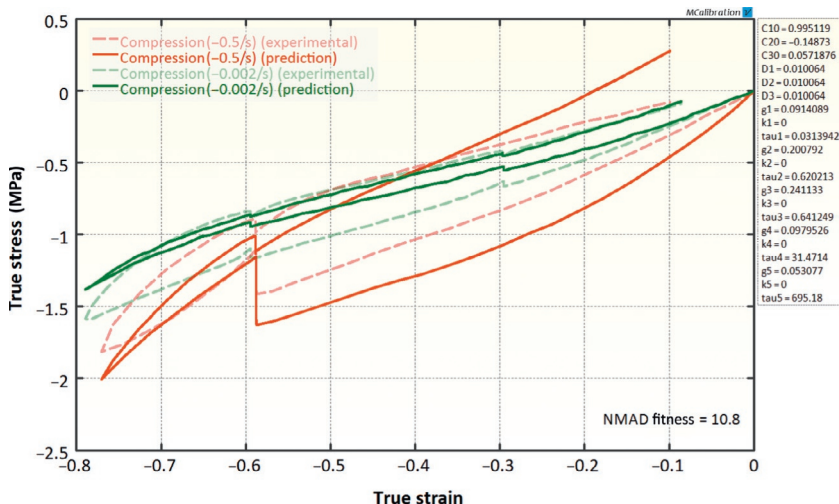


Figure 11.9 Comparison between experimental data for CR and the best model predictions from a linear viscoelastic model.

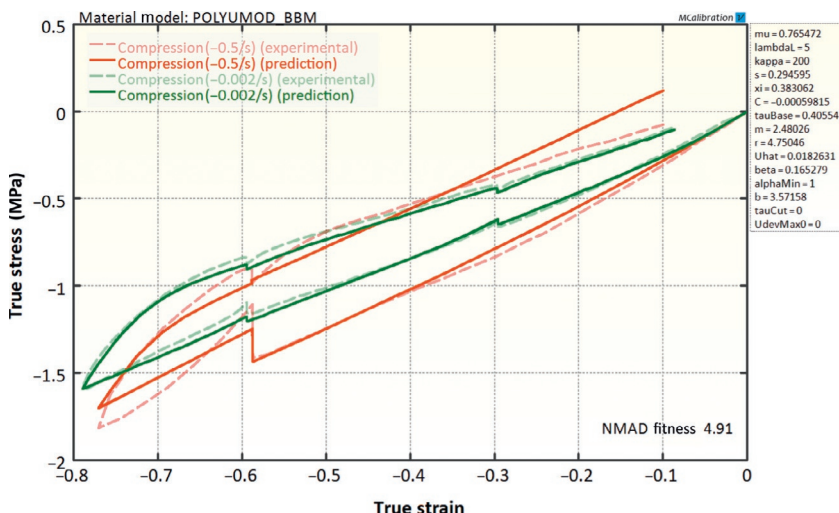


Figure 11.10 Comparison between experimental data for CR and the best model predictions from the BB model with Mullins damage.

Adding one additional viscoelastic network to the BB model increases the accuracy to 4.2%. Adding further networks does not further improve the accuracy in any significant way. Also for this elastomer the TN model is less accurate than the BB model due to the lack of a flow equation with strain dependence.

11.4 Nitrile Rubber

Nitrile rubber, which is also called Buna-N or NBR, is an unsaturated synthetic copolymer. It is commonly used to make hoses, seals, gloves, and many other industrial products. The mechanical response of nitrile rubber can be tested in many different ways. The example shown here used uniaxial compression at different strain rates and strain cycles. Figures 11.11 and 11.12 depict the mechanical response at three strain rates (-0.5 , -0.1 , and $-0.01/s$). In each test, multiple stress relaxation segments were inserted. The slow strain rate test had 14 stress relaxation segments inserted, each 300 s long. The two faster tests had 30 s long stress relaxation segments. As is typically seen with rubbers, the stress magnitude goes down during the stress relaxation during the loading phase, and the stress magnitude goes up during the stress relaxation during the unloading phase (Table 11.3).

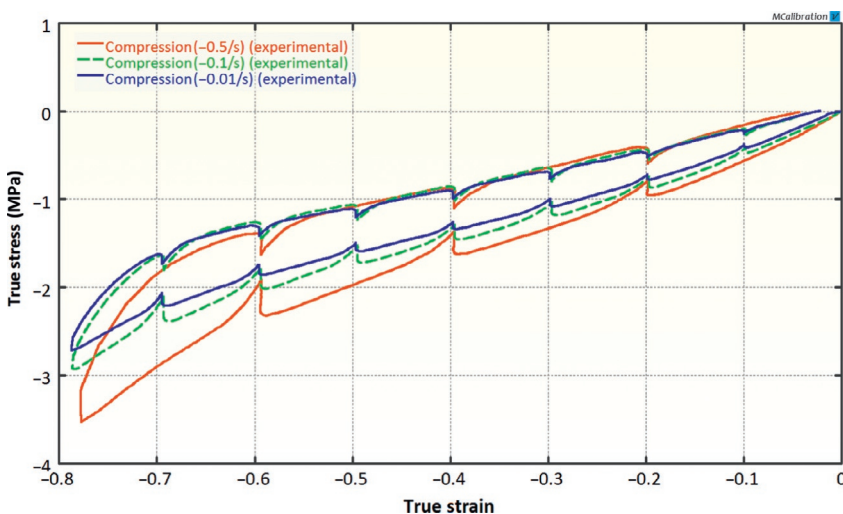


Figure 11.11 Uniaxial compression data for a nitrile rubber.

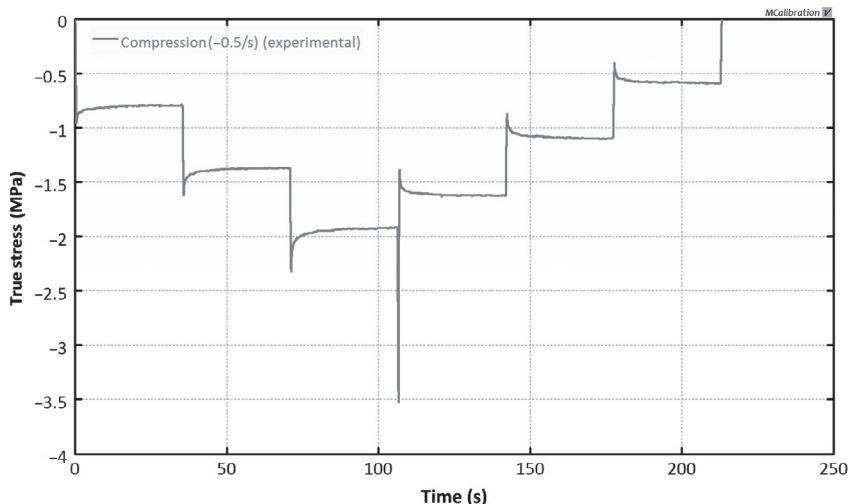


Figure 11.12 Stress-time response of the nitrile rubber tested at a true strain rate of $-0.5/\text{s}$.

Table 11.3 Summary of Results from Material Model Calibrations of the Nitrile Rubber

Material Model	Error in Model Calibration (%)
Arruda-Boyce eight-chain	17.7
Yeoh	17.1
Linear viscoelasticity (Yeoh)	9.8
BB	5.3
BB with Mullins damage	4.6
Higher order Parallel Network models with Mullins damage	4.6

Like the other two elastomers discussed in this chapter, nitrile rubber exhibits significant viscoelasticity and hysteresis making hyperelastic models unable to capture the experimental response. Figure 11.13 shows that hyperelastic models have an error of

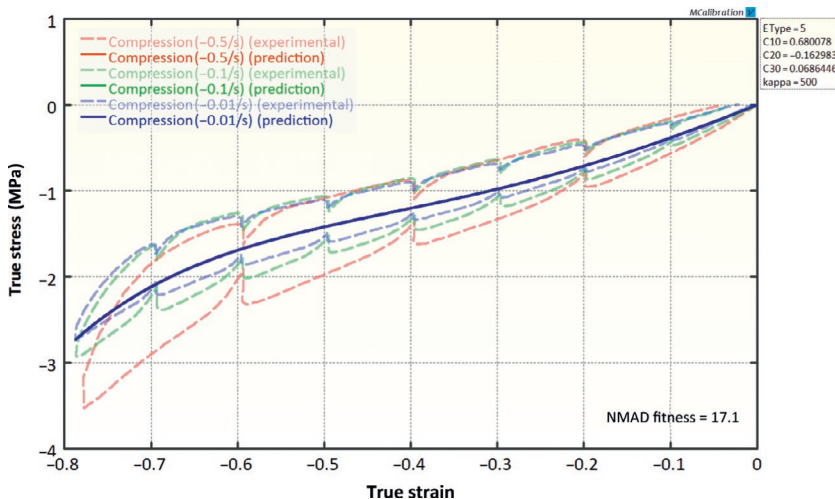


Figure 11.13 Comparison between experimental data for nitrile rubber and the best model predictions from the Yeoh hyperelastic model.

approximately 17% (calculated using the NMAD error defined in Equation (9.5)).

The next step after trying a hyperelastic model is to examine a linear viscoelastic material model. Figure 11.14 shows a comparison between the experimental data for the nitrile rubber and the best predictions from a linear viscoelastic material model based on Yeoh hyperelasticity and a five-term Prony series representation. Since the material response is nonlinear viscoelastic, a linear viscoelastic model cannot accurately represent the material response. The average error is about 9.0%.

The stress-strain response of the nitrile rubber can be accurately represented using the BB model (Section 8.2) with Ogden-Roxburgh Mullins damage (Section 5.7.1). This model accurately represents the material response. The average error of the predictions is about 4.6% (as determined by the NMAD fitness value). The original BB model without Mullins damage in this case has an error of about 5.3%. Adding additional nonlinear viscoelastic networks to the material model framework does not improve the predicted accuracy (Figure 11.15).

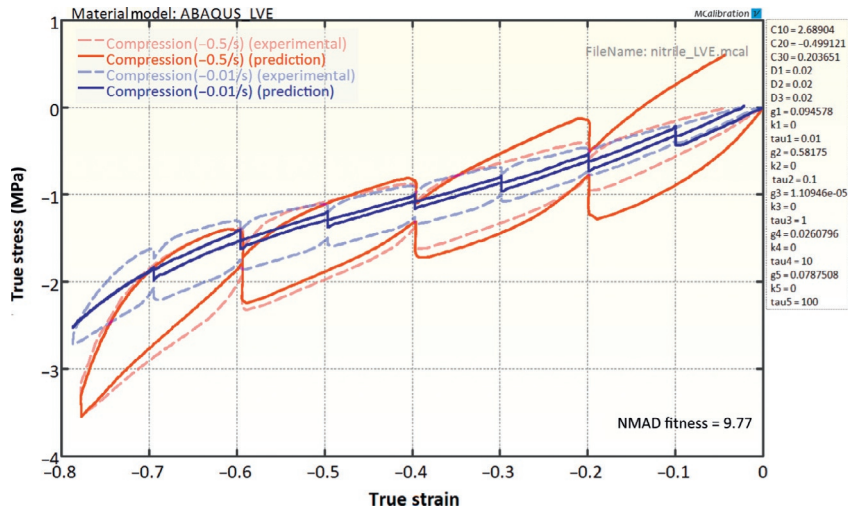


Figure 11.14 Comparison between experimental data for nitrile rubber and the best model predictions from a linear viscoelastic material model based on Yeoh hyperelasticity. The linear viscoelastic model was based on a five-term Prony series.

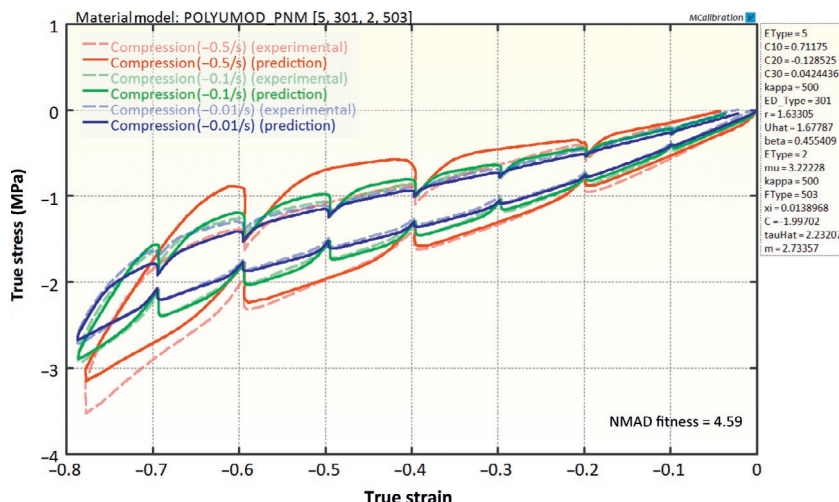


Figure 11.15 Comparison between experimental data for nitrile rubber and the best model predictions from the BB model with Mullins softening.

11.5 Santoprene

Santoprene is a thermoplastic vulcanizates (TPV) consisting of EPDM rubber particles inside a polypropylene (PP) matrix. Due to this combination, Santoprene has properties that are similar to both elastomers and thermoplastics. [Figure 11.16](#) shows uniaxial tensile stress-strain data at three different strain rates. One of the tests in this figure contained 10 load-unload cycles at intermediate strains. [Figure 11.17](#) shows the results of another cyclic loading experiment on the same material. In this case, the strain was held constant for 10 min at three strain levels. The relaxation segments, indicated by red lines in the figure, show that the material undergoes significant relaxation when the strain is held constant.

The accuracy of many different material models to represent the experimental data of the Santoprene are examined in this section. [Table 11.4](#) summarizes the findings.

[Figure 11.18](#) shows that a hyperelastic material model cannot represent the viscoplastic response of a Santoprene. This figure shows that a Yeoh hyperelastic model has an average error in

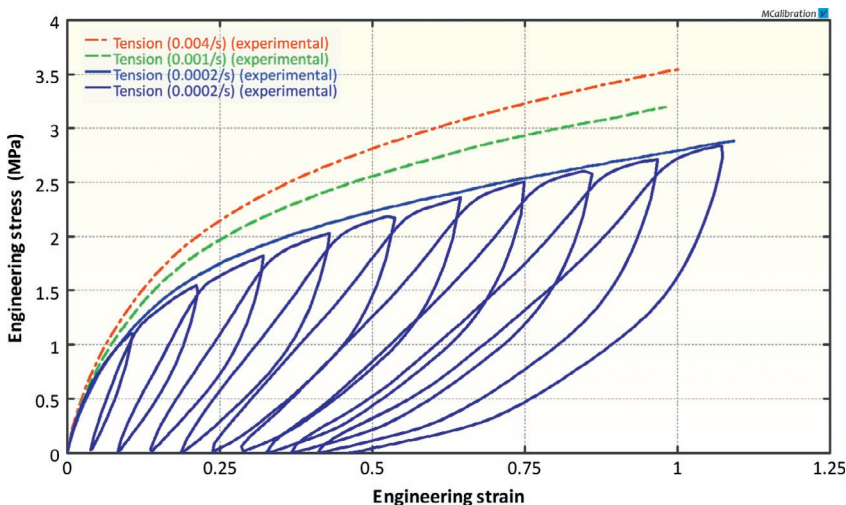


Figure 11.16 Uniaxial tension data for a Santoprene at three different strain rates.

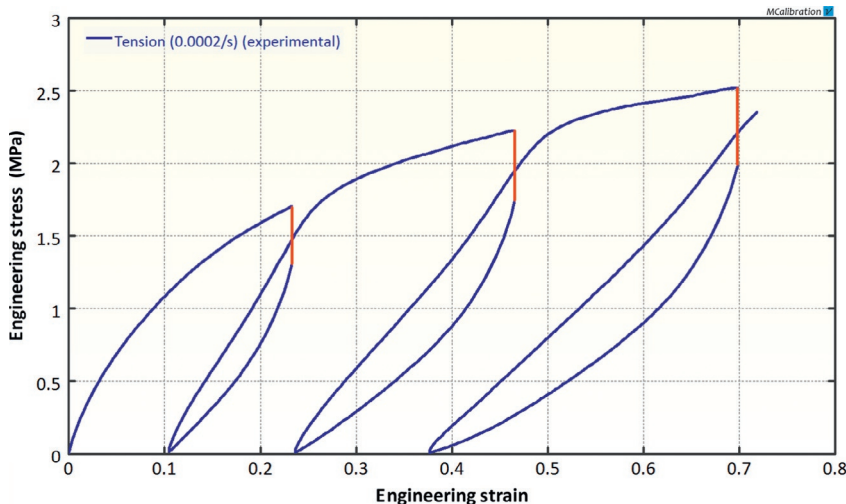


Figure 11.17 Uniaxial tension data for a Santoprene. The red-line segments show the stress relaxation behavior at three strain levels.

the stress-strain predictions of about 41%. Hence, all hyperelastic models are inadequate for anything but the most basic FE study.

LVE is a more promising candidate model framework, see [Figure 11.19](#)). The LVE model is here based on Yeoh hyperelasticity and a five-term Prony series. The average error of the model predictions is 16.3%.

Since the matrix material of Santoprene is PP it is worthwhile to examine the utility of metal plasticity models. [Figure 11.20](#) shows the predictions from an isotropic hardening plasticity model with rate-dependence. Specifically, the following Abaqus keywords were used:

```
*Elastic
*Plastic, hardening=isotropic
*Rate Dependent, type=power law
```

The average error of the model calibration is 18%.

In this example, the material is exposed to cyclic loading, it is therefore more appropriate to use a kinematic hardening plasticity model. [Figure 11.21](#) shows the predicted response of an elastic-plastic material model with combined kinematic hardening and one backstress network. The average error of this model is 19%.

Table 11.4 Summary of Results from Material Model Calibrations for Santoprene

Material Model	Error in Model Calibration (%)
Arruda-Boyce eight-chain	42.5
Yeoh	38.8
Elastic-plastic with kinematic hardening (one backstress network)	18.6
Elastic-plastic with isotropic hardening and rate-dependence	17.6
Linear viscoelasticity (Yeoh)	16.3
Three Network model	9.8
Dual Network Fluoropolymer (DNF) model	9.5
Elastic-plastic with kinematic hardening and rate-dependence (three backstress networks)	9.0
BB	7.5
BB with Mullins damage	5.6
Parallel Network model with three networks of BB type and Mullins damage	2.7
Parallel Network model with four or more networks of BB type and Mullins damage	2.7

The accuracy of the material model can be enhanced by using three backstress networks and including plastic strain creep. As shown in [Figure 11.22](#), the average of this model is 9.0%.

A completely different modeling approach is provided by the BB model, and multi-network versions of this model. [Figure 11.23](#) shows that the basic BB model captures the experimental data reasonably well with an average error of the predictions of 7.5%. This quality of the predictions of this model can be strengthened by including Mullins damage through the

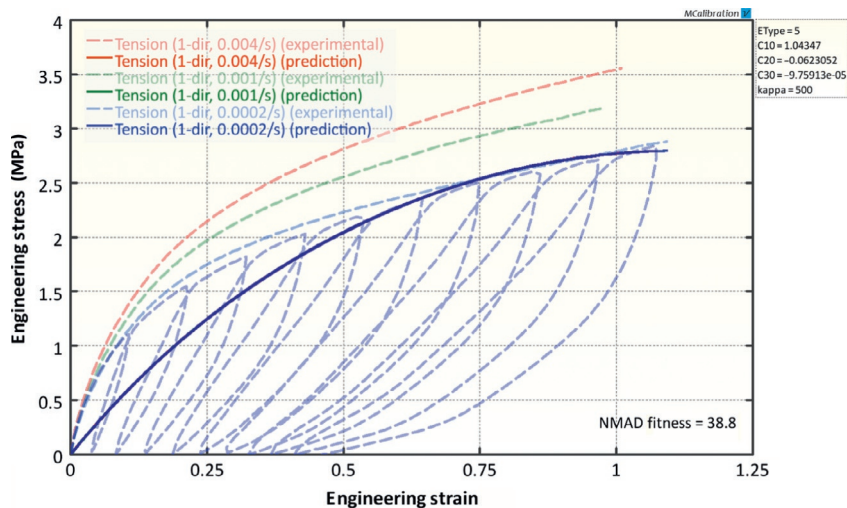


Figure 11.18 Comparison between experimental data for Santoprene and the best model predictions from the Yeoh hyperelastic model.

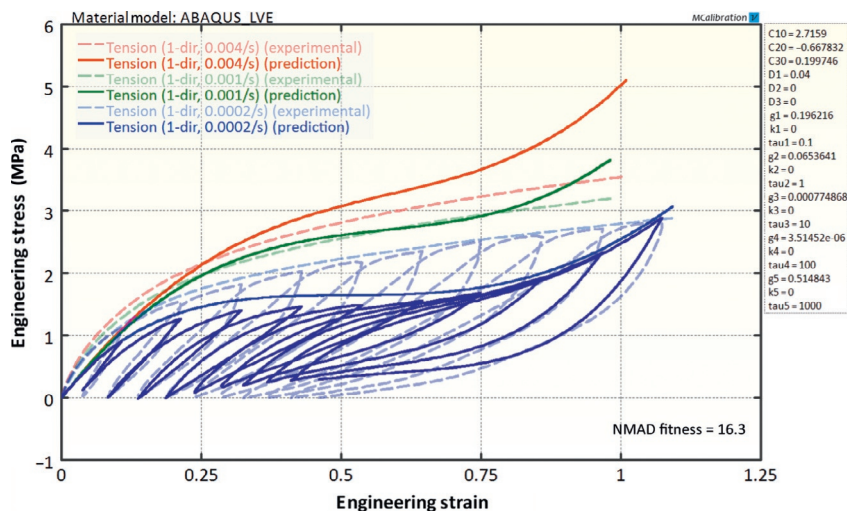


Figure 11.19 Comparison between experimental data for Santoprene and the best model predictions from a linear viscoplastic model.

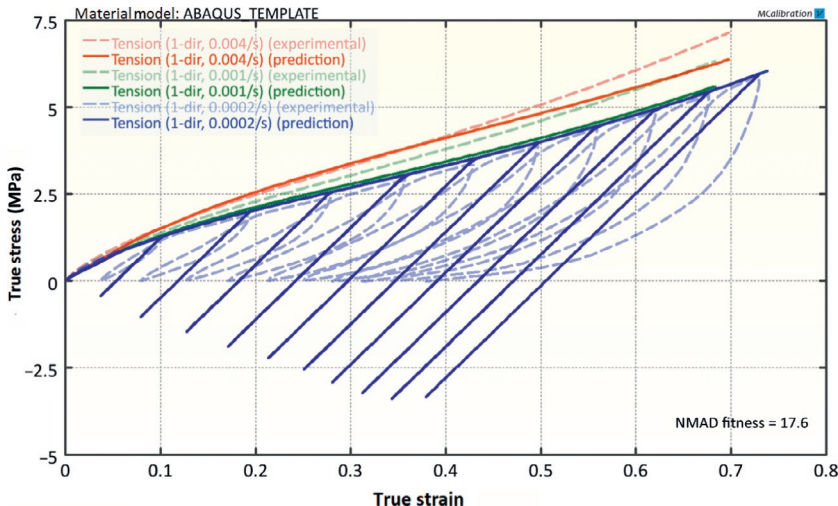


Figure 11.20 Comparison between experimental data for Santoprene and the best model predictions from an elastic-plastic material model with isotropic hardening and rate-dependence.

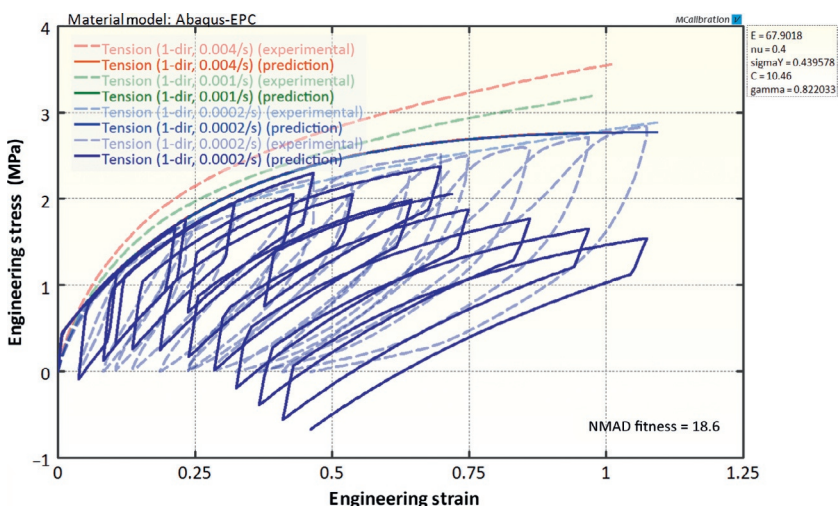


Figure 11.21 Comparison between experimental data for Santoprene and the best model predictions from an elastic-plastic material model with combined kinematic hardening and one backstress network.

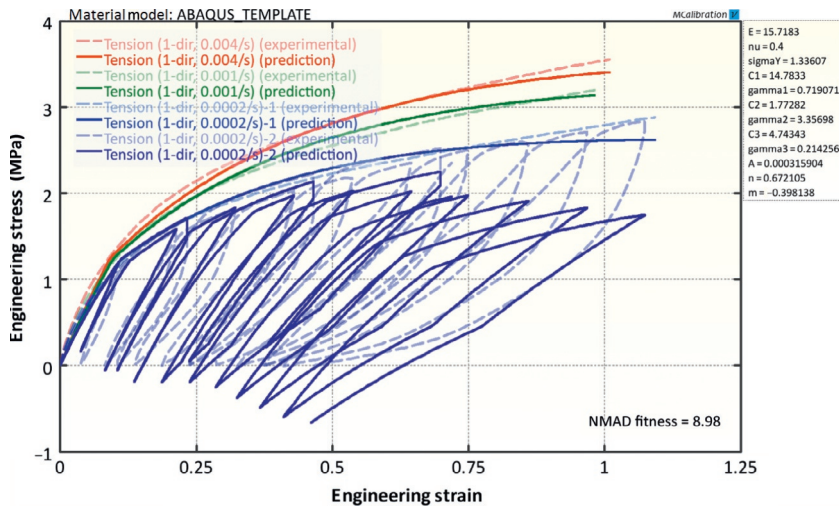


Figure 11.22 Comparison between experimental data for Santoprene and the best model predictions from an elastic-plastic material model with combined kinematic hardening, plastic creep, and three backstress networks.

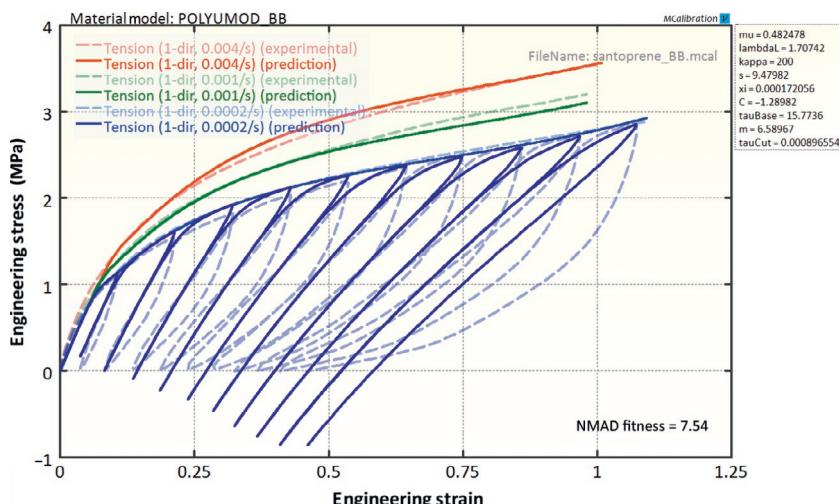


Figure 11.23 Comparison between experimental data for Santoprene and the best model predictions from the BB model.

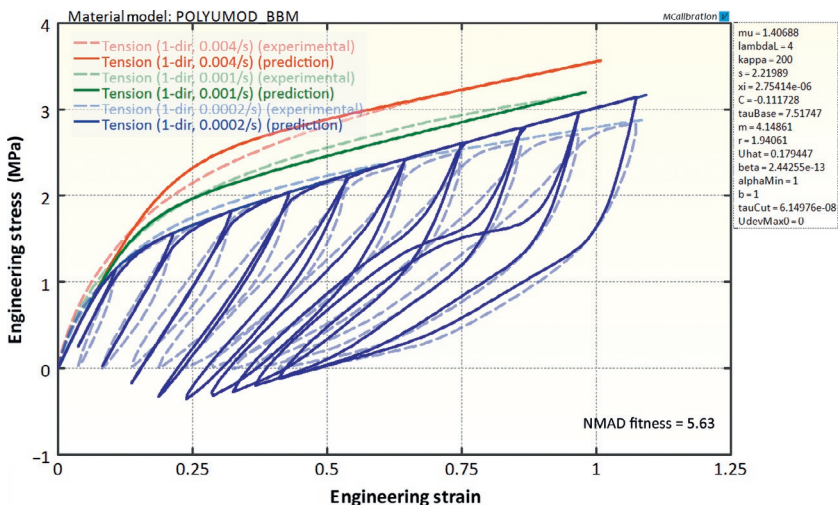


Figure 11.24 Comparison between experimental data for Santoprene and the best model predictions from the BB model with Mullins damage.

Ogden-Roxburgh approach. Figure 11.24 illustrates a significantly improved visual appearance of the predicted response. The average error for this model is 5.6%.

The most accurate material model in this case is the three network extension of the BB model with Mullins damage. That is, the model framework consists of three parallel networks where the first network is a simple Yeoh hyperelastic network, the second and third networks consist of a Neo-Hookean spring in series with a BB viscoplastic flow element. The predicted response of this model is shown in Figures 11.25 and 11.26. The average error of this model calibration is 2.7%.

11.6 High-Density Polyethylene

High-density polyethylene (HDPE) is a semicrystalline polymer that is commonly used in both industrial and consumer products. The mechanical response of HDPE is similar to many soft thermoplastics in that it starts to undergo viscoplastic deformations at very small strains. Figure 11.27 shows the stress-

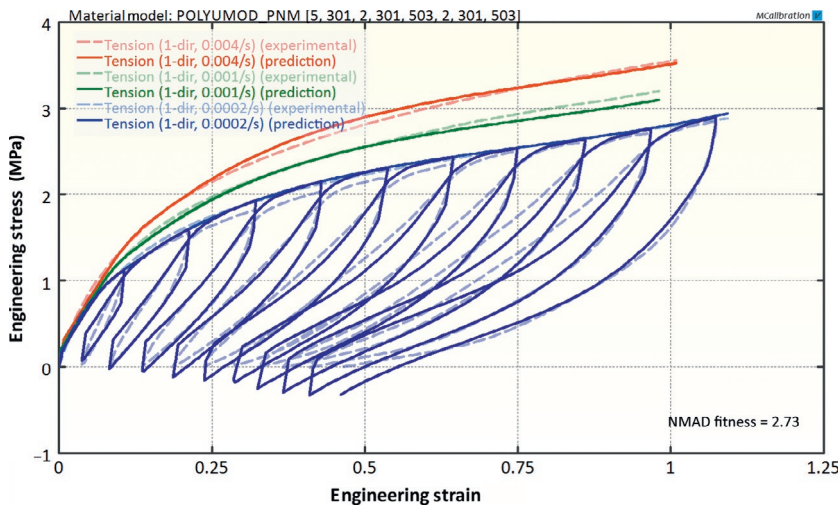


Figure 11.25 Comparison between experimental data for Santoprene and the best model predictions from the PN model with three networks with BB type flow and Mullins damage.

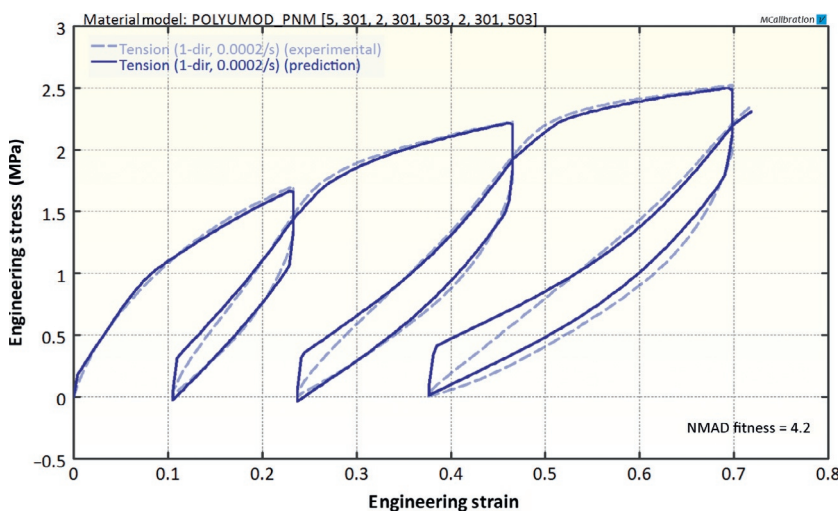


Figure 11.26 Comparison between experimental data for Santoprene and the best model predictions from the PN model with three networks with BB type flow and Mullins damage.

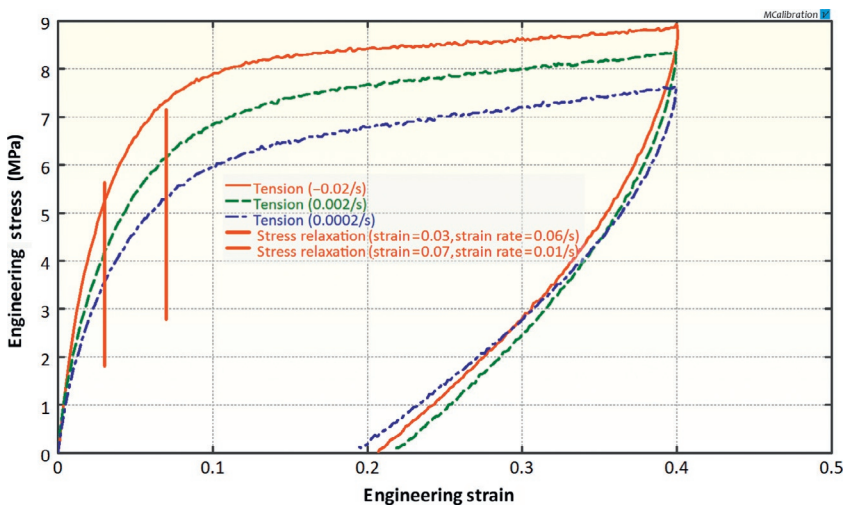


Figure 11.27 Uniaxial tension data for a HDPE.

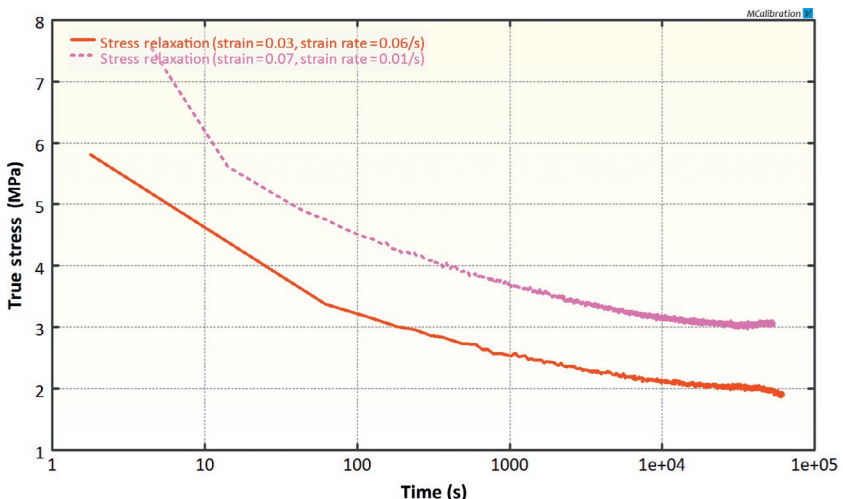


Figure 11.28 Stress relaxation data for a HDPE.

strain response of a HDPE tested in uniaxial tension at three different strain rates. The figure also shows the stress relaxation response when loaded to 3% and 7% engineering strain for 15 h. Under these conditions the stress relaxes by more than 50% (Figure 11.28).

Table 11.5 Summary of Results from Material Model Calibrations for HDPE

Material Model	Error in Model Calibration (%)
Elastic-plastic with isotropic hardening and rate-dependence	58.5
Arruda-Boyce eight-chain	38.1
Yeoh	27.2
Linear viscoelasticity (Yeoh)	37.2
BB	8.0
Parallel Network model with two networks (Power flow)	7.9
Elastic-plastic with kinematic hardening and rate-dependence (three backstress)	7.8
DNF model	7.6
Three Network model	5.2
Parallel Network model with three networks (Power flow)	5.0
Parallel Network model with four networks (Power flow)	4.8
Parallel Network model with five networks (Power flow)	4.7

As is summarized in [Table 11.5](#), there are many different candidate material models than can be used to model the response of HDPE with varying degree of success.

As a first example, [Figure 11.30](#) presents the predictions from an elastic-plastic material model with isotropic hardening and a yield stress that depends on the plastic strain rate (see Section 7.2). This material model can represent the monotonic tension response at different strain rates, but since it is based

on isotropic hardening the unloading response is quite inaccurate (Figure 11.29).

Similarly, a hyperelastic material model is not adequate for HDPE. Figure 11.30 illustrates that the Arruda-Boyce eight-chain model is not suitable for HDPE.

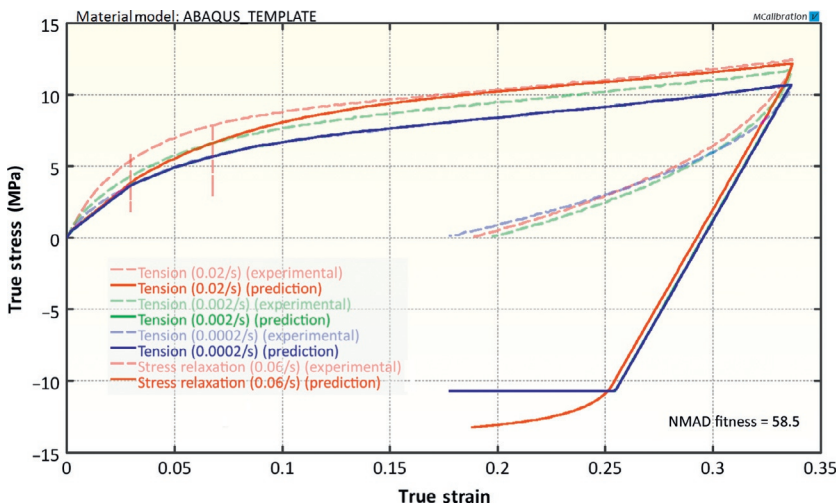


Figure 11.29 Comparison between experimental data for HDPE and the best model predictions from an elastic-plastic material model with combined kinematic hardening and one backstress network.

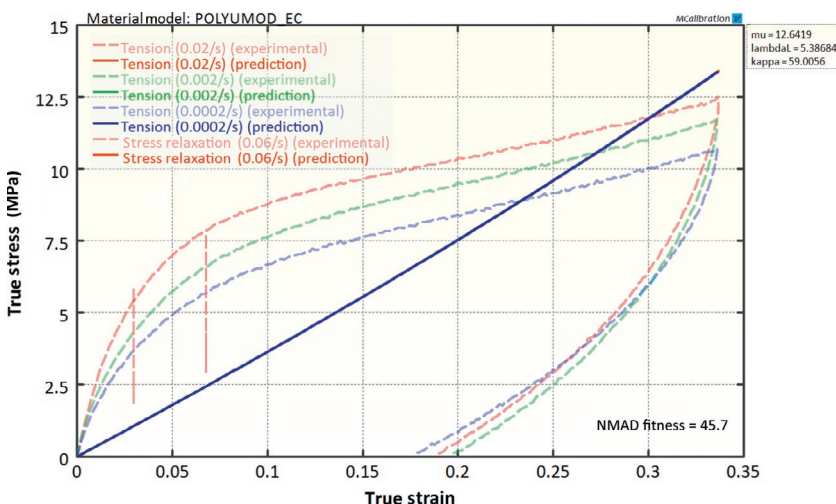


Figure 11.30 Comparison between experimental data for HDPE and the best model predictions from the Arruda-Boyce eight-chain model.

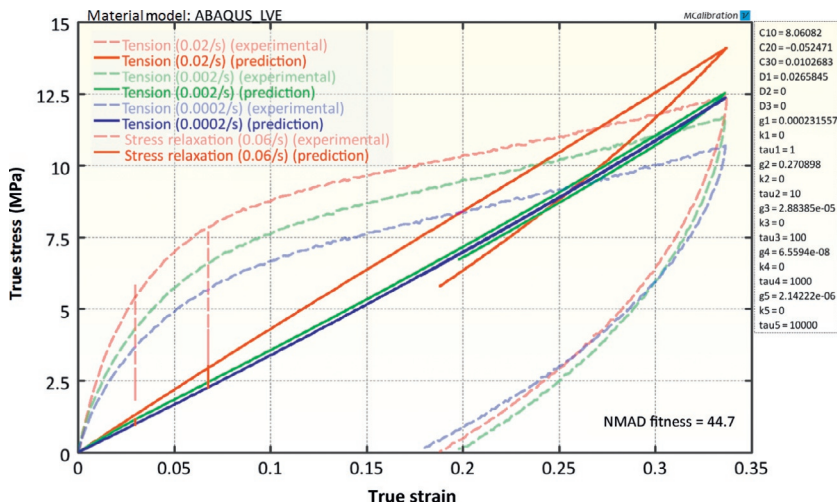


Figure 11.31 Comparison between experimental data for HDPE and the best model predictions from a linear viscoplastic model.

Due to the large amount of plastic deformation that occurs in the material at finite deformations it is not possible to use a linear viscoelastic material model for the HDPE data (see Figure 11.31).

The experimental data for the HDPE can be accurately captured using the PN model (see Section 8.7). Figures 11.32–11.35 demonstrate that the accuracy of the model calibration increases with increasing number of networks in the model representation. In this example, the hyperelastic components of the PN model were taken as Yeoh elements, and the viscoplastic flow elements were taken as a simple Power-flow model (see Equation (8.31)).

11.7 Polytetrafluoroethylene

Polytetrafluoroethylene (PTFE) is a solid fluorocarbon polymer containing only carbon and fluorine. PTFE has a lower friction coefficient than most other materials, and it has excellent dielectric properties. It is commonly used in many industrial and medical device applications.

The mechanical behavior of PTFE is characterized by significant nonlinearities in terms of applied loading rates and loading

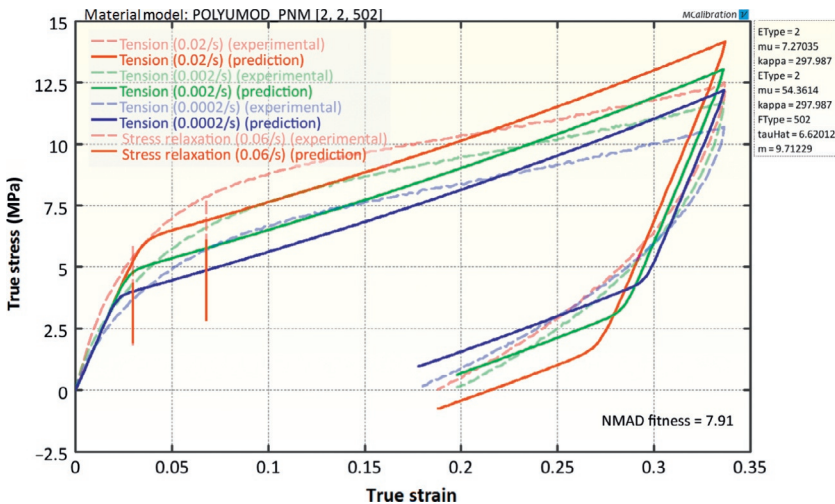


Figure 11.32 Comparison between experimental data for HDPE and the best model predictions from the PN model with two networks with Power-law type flow.

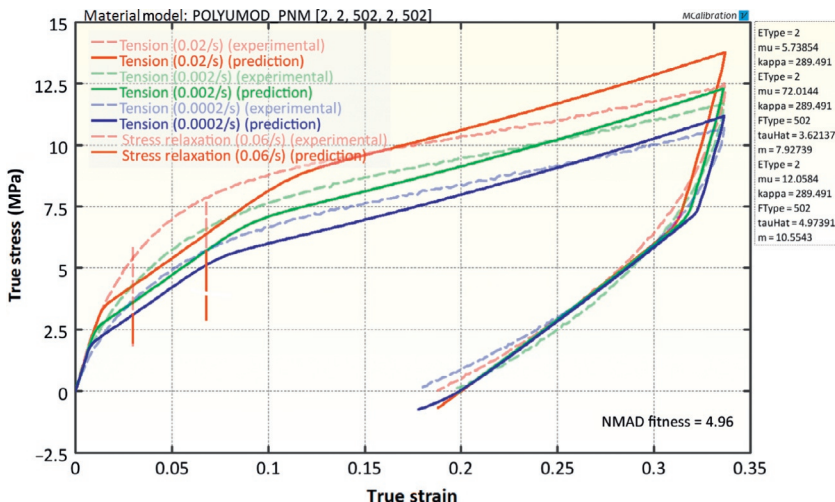


Figure 11.33 Comparison between experimental data for HDPE and the best model predictions from the PN model with three networks with Power-law type flow.

history. Figures 11.36–11.38 show stress-strain data for a PTFE material filled with 10 vol% glass fibers [1]. As is typical for PTFE the yield stress is significantly higher in compression than in tension. This difference in behavior between tension and

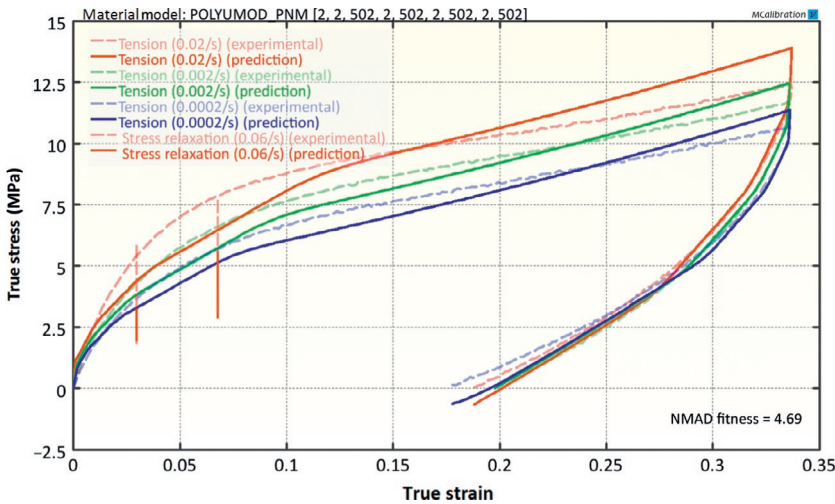


Figure 11.34 Comparison between experimental data for HDPE and the best model predictions from the PN model with five networks with Power-law type flow.

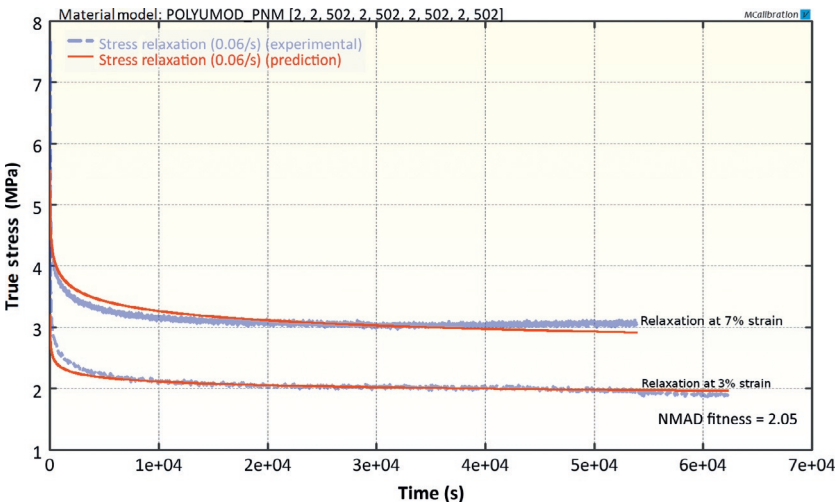


Figure 11.35 Comparison between experimental data for HDPE and the best model predictions from the PN model with five networks with Power-law type flow.

compression is partly caused by a small amount of microporosity that is characteristic of PTFE. These figures also show that both the deviatoric and volumetric response undergoes viscoplastic relaxation under the tested conditions.

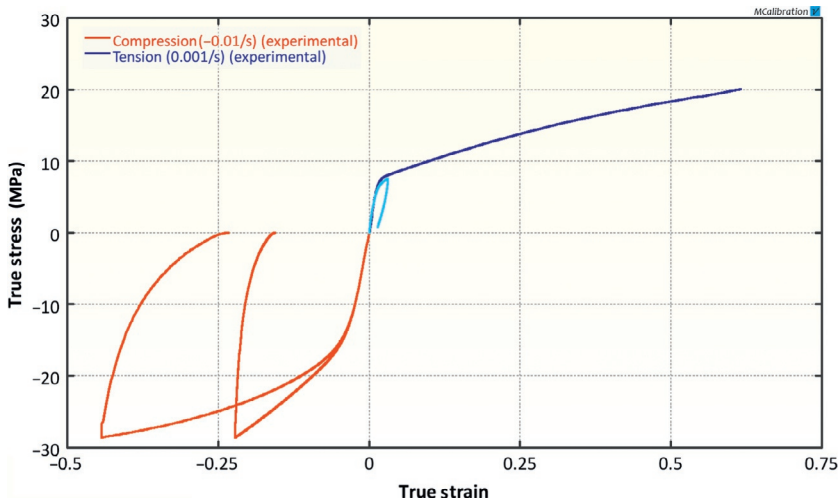


Figure 11.36 Uniaxial tension and compression data for a PTFE material. The yield stress is higher in compression than in tension.

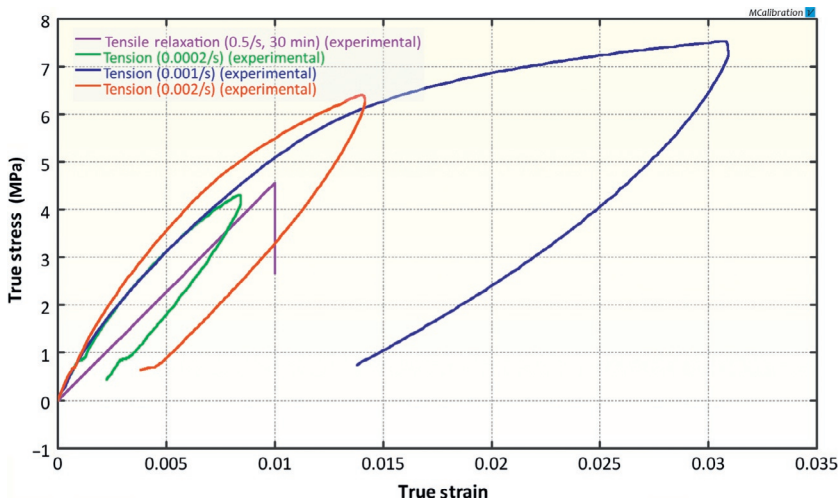


Figure 11.37 Uniaxial tension data for a PTFE material tested at multiple strain rates. The tests include loading, unloading, and stress relaxation segments.

The predictive capabilities of a number of different candidate material models are summarized in [Table 11.6](#).

This comprehensive experimental data set containing both tension and compression data at different strain rates is challenging for many material models to capture. An elastic-plastic

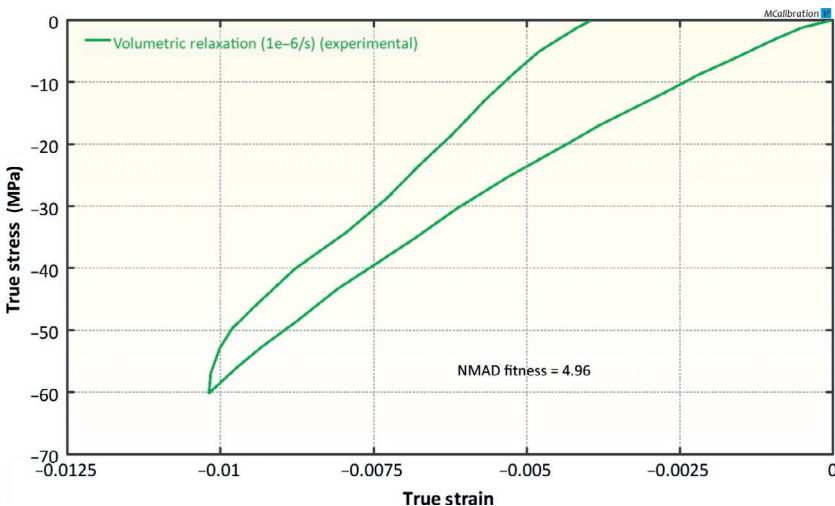


Figure 11.38 Volumetric compression data for a PTFE material.

material model, in this case without strain-rate dependence, is clearly unable to represent the material response as shown in [Figure 11.39](#). One of the main issues with this material model is that it is unable to distinguish between flow resistance in tension and compression. Note that all experimental data and model predictions are plotted in the same graph in order to get one comprehensive view of the data.

A significantly more accurate representation of the data is achieved by a two-network PN model where each network consists of a Neo-Hookean hyperelastic component in series with a Power-law flow element with pressure dependence. The predictions of this model are shown in [Figure 11.40](#). The average error in the model predictions is 16%.

An elastic-plastic material model with combined kinematic hardening and creep-based rate-dependence captures the experimental data surprisingly well in this case. As shown in [Figure 11.41](#), this model has an average error of about 16.3%.

The DNF model is specifically designed for fluoropolymers and as shown in [Figure 11.42](#) reasonably accurately captures the complete experimental data setup for the fiber filled PTFE. The main limitation of the DNF model is that it under predicts

Table 11.6 Summary of Results from Material Model Calibrations for HDPE

Material Model	Error in Model Calibration (%)
Neo-Hookean	79.0
Arruda-Boyce eight-chain	72.0
Linear viscoelasticity (Yeoh)	52.5
Yeoh	49.6
Elastic-plastic with isotropic hardening	32.7
ANSYS Chaboche with Perzyna rate-dependence	29.0
BB	19.7
Parallel Network model with two networks (Power flow)	16.4
Elastic-plastic with kinematic hardening and rate-dependent creep (three backstress)	16.3
DNF model	14.8
Parallel Network model with three networks (Power flow)	14.0
Parallel Network model with four networks (Power flow)	13.5
Three Network model	10.8

the recovery during unloading. The average error in the model predictions is 15%.

The most accurate material model for the PTFE data is the TN model. [Figure 11.43](#) shows that the TN model provides an overall accurate representation of all aspects of the stress-strain response of the PTFE in this study. The average error of the TN model predictions is 10.8%.

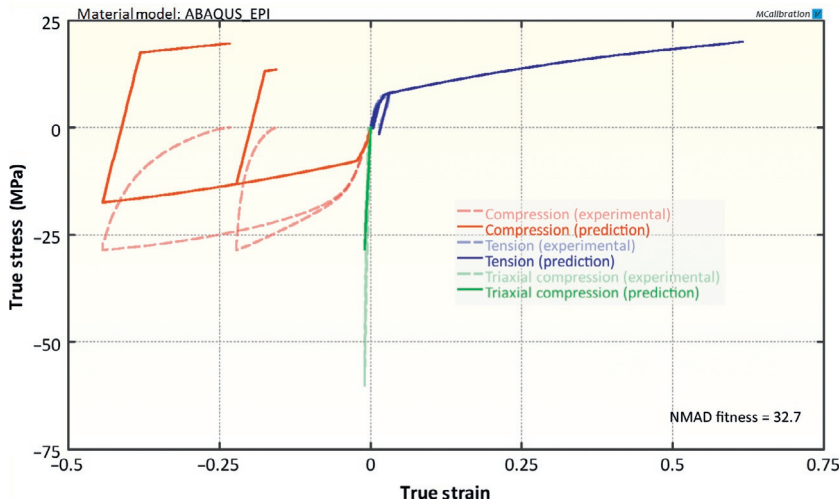


Figure 11.39 Comparison between experimental data for PTFE and the best model predictions from an elastic-plastic material model with isotropic hardening.

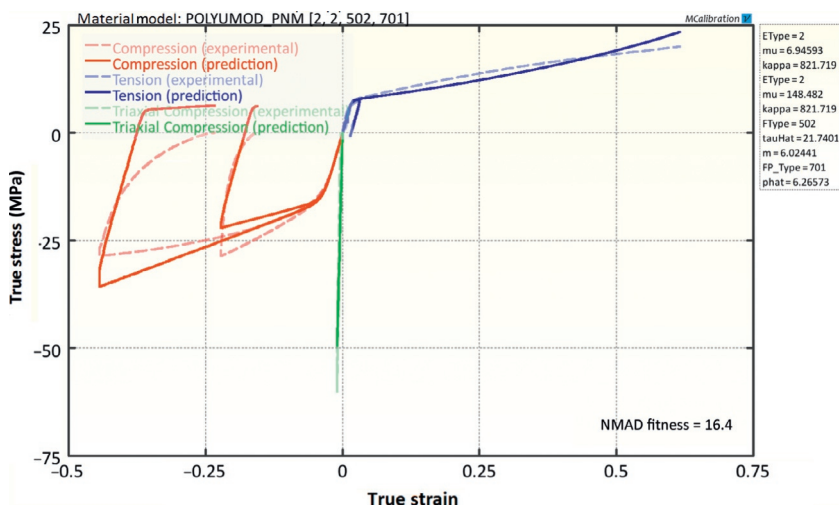


Figure 11.40 Comparison between experimental data for PTFE and the best model predictions from a two-network PN model.

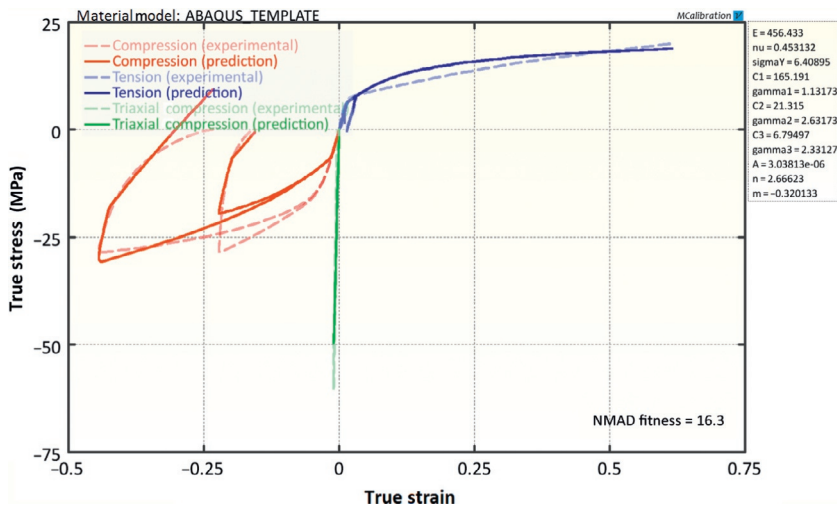


Figure 11.41 Comparison between experimental data for PTFE and the best model predictions from the Abaqus elastic-plastic material model with combined kinematic hardening and creep-based rate-dependence. The model has three backstress networks.

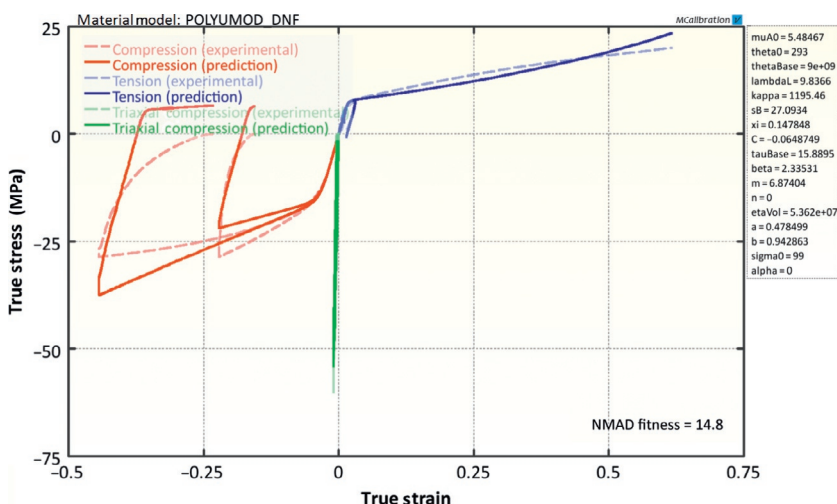


Figure 11.42 Comparison between experimental data for PTFE and the best model predictions from the DNF model.

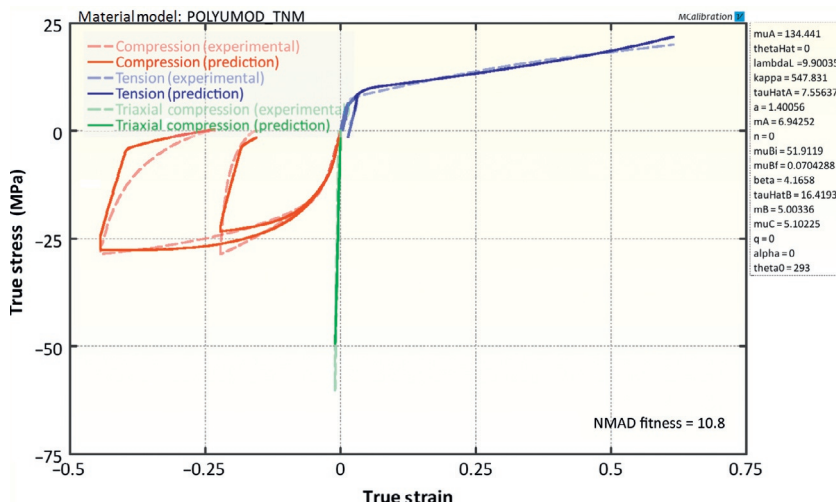


Figure 11.43 Comparison between experimental data for PTFE and the best model predictions from the TN model.

11.8 Polyethylene Terephthalate

Polyethylene terephthalate (PET) is a thermoplastic polyester that is often used in synthetic fibers, bottles, and containers. PET can be either amorphous or semi-crystalline depending on the thermal history. Experimental tension data for a PET material is shown in Figure 11.44 [2]. This figure shows that the stress-strain response is strain-rate dependent and that the true stress softens significant after the initial peak value. At large strains the stress starts to increase again due to molecular alignment.

The predictive capabilities of a number of different candidate material models are summarized in Table 11.7.

The best calibration of the BB model to the experimental data is shown in Figure 11.45. As expected, the BB model is unable to represent the stress reduction after the initial peak stress. The overall average error in the calibration results is 5.9%.

A significantly more accurate prediction is provided by an elastic-plastic material model with isotropic hardening and rate-dependent yield stress (see Figure 11.46). This model does a good job at reproducing the overall shape of the stress-strain response, but as was discussed in Section 7.2, it should not

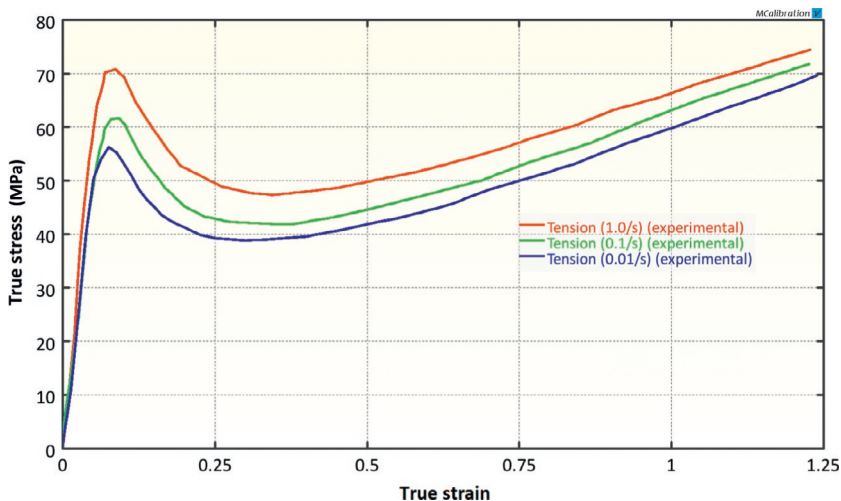


Figure 11.44 Uniaxial tension data at three different strain rates for a PET material.

Table 11.7 Summary of Results from Material Model Calibrations for HDPE

Material Model	Error in Model Calibration (%)
Arruda-Boyce eight-chain	41.2
Yeoh	25.9
Linear viscoelasticity (Yeoh)	26.3
BB	19.7
Abaqus elastic-plastic with isotropic hardening and creep	7.1
Abaqus elastic-plastic with isotropic hardening and rate dependence	3.8
Parallel Network model with two networks (yield evolution)	2.4
Three Network model	2.4

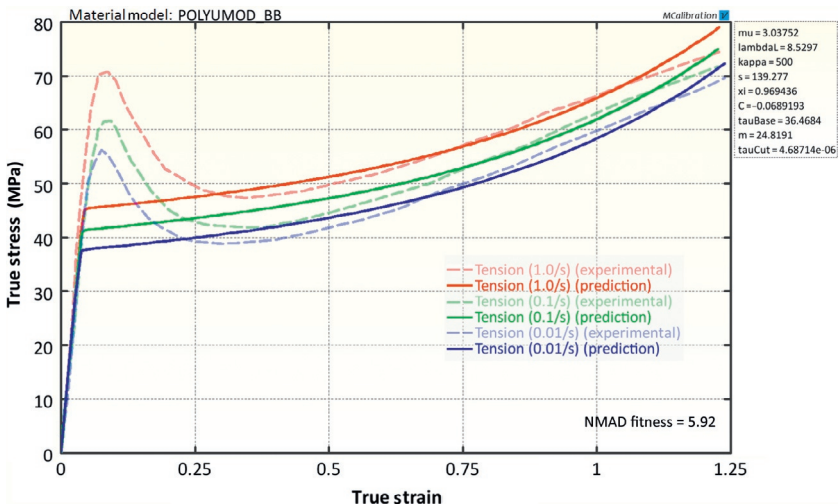


Figure 11.45 Comparison between experimental data for PET and the best model predictions from the BB material model.

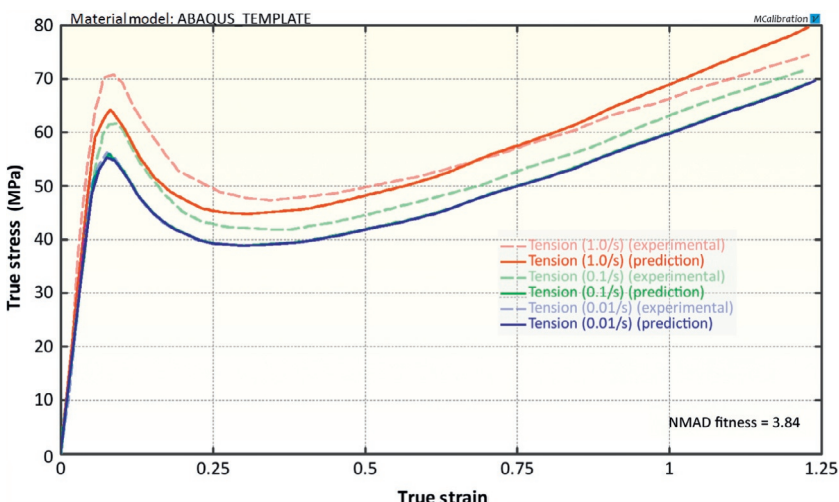


Figure 11.46 Comparison between experimental data for PET and the best model predictions from Abaqus elastic-plastic model with isotropic hardening and rate-dependence.

be used in applications where the applied load also includes unloading.

The most accurate material model for this material was found to be the TN model. [Figure 11.47](#) shows that the TN model represents the experimental data with great accuracy.

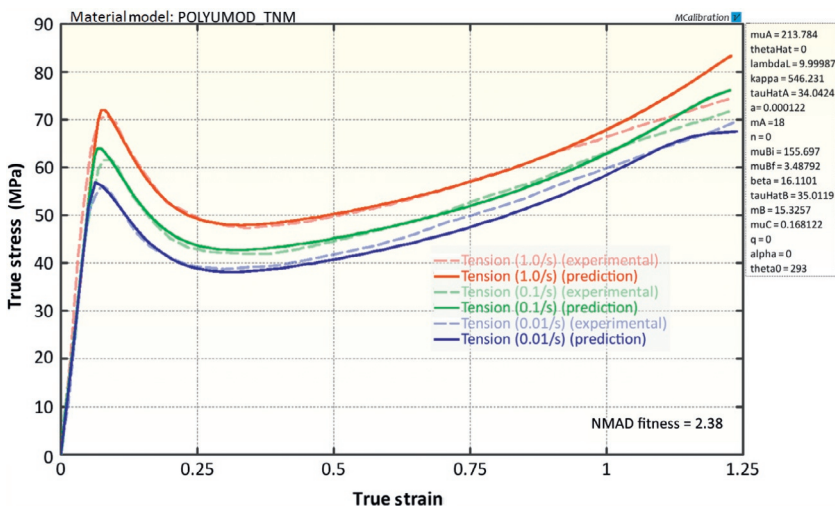


Figure 11.47 Comparison between experimental data for PET and the best model predictions from the TN model.

11.9 Polyether Ether Ketone

Polyether ether ketone (PEEK) is a high strength and stiffness semicrystalline thermoplastic. Due to its excellent mechanical properties it is commonly used in seals and bearings, and more recently also in medical implants (e.g., spinal implants, screws, woven textiles).

Experimental data for a PEEK material is shown in [Figure 11.48](#). This figure summarizes uniaxial tension data at two strain rates (0.1 and 0.001/s), and uniaxial compression data at strain rates of -1000 , -0.1 , and $-0.004/s$. The response at $-1000/s$ was obtained using a split Hopkinson pressure bar testing (see Section 2.2.8). The data illustrate that the material has slightly higher yield stress in compression than in tension, and that the stress-strain response after unloading is highly nonlinear.

The predictive capabilities of a number of different candidate material models are summarized in [Table 11.8](#). The large error in the elastic-plastic model with isotropic hardening and rate-dependent plastic flow is a results of the calibration procedure. First, the plasticity parameters were determined from the large strain tension results, then the rate-dependence parameters were found in order to best match the complete data set.

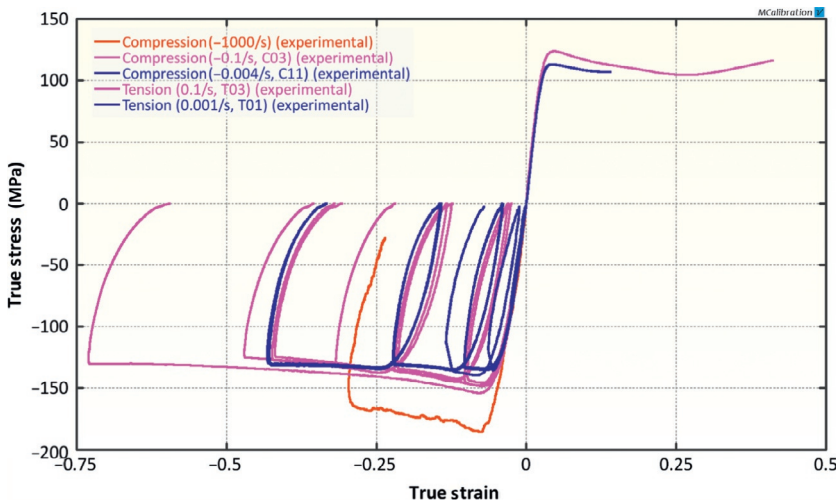


Figure 11.48 Uniaxial tension and compression data for an unfilled PEEK material.

The best calibration of the BB model to the experimental data for PEEK is shown in Figure 11.49. As expected, the BB model captures the overall response of the material reasonably well, but is unable to accurately represent the nonlinear stress response after unloading. The average error in the calibration results is 24.3%.

The Johnson-Cook (JC) plasticity model (see Section 7.4) is similar to the BB model in its predictive capabilities of the PEEK data. Also in this case the main limitation of the predictions is the linear stress response during unloading. The average error in the calibration results is 24.9% (Figure 11.50).

The PN model has the advantage that it allows for suitable components to be selected. In this case, an appropriate starting point is a two-network representation where network 1 has a Neo-Hookean element, and where network 2 has a Neo-Hookean element to represent the elastic response and a Power-law flow element (Equation (8.68) with yield evolution (Equation (8.69)) and pressure dependence of the yield stress (similar to the a parameter in Equation (8.64))). The calibration results from this model is shown in Figure 11.51. The predictions are in reasonable agreement with the experimental data, and the average error in the

Table 11.8 Summary of Results from Material Model Calibrations for PEEK

Material Model	Error in Model Calibration (%)
Elastic-plastic with isotropic hardening and rate-dependence	127
Arruda-Boyce eight-chain	68.4
Yeoh	59.6
DNF	30.9
Elastic-plastic with kinematic hardening and rate-dependent creep (three backstress)	30.6
Johnson-Cook	24.8
BB	24.4
Parallel Network model with two networks (Power flow, yield evolution, pressure dependence)	16.5
Parallel Network model with three networks (Power flow, yield evolution, pressure dependence)	9.1
Three Network model	9.1

calibration results is 16.5%. The accuracy of this model framework can be improved further by adding one more viscoelastic network of similar type.

The TN model accurately predicts the response of the PEEK at all tested conditions, see [Figure 11.52](#). The stress-strain response may look somewhat multilinear due to the small number of mechanisms used to represent the material response. The average error of the model predictions is 9.1%.

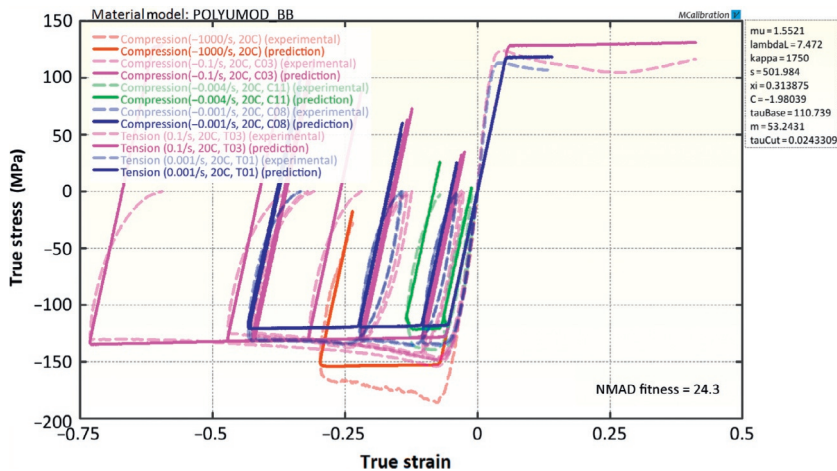


Figure 11.49 Comparison between experimental data for PEEK and the best model predictions from the BB material model.

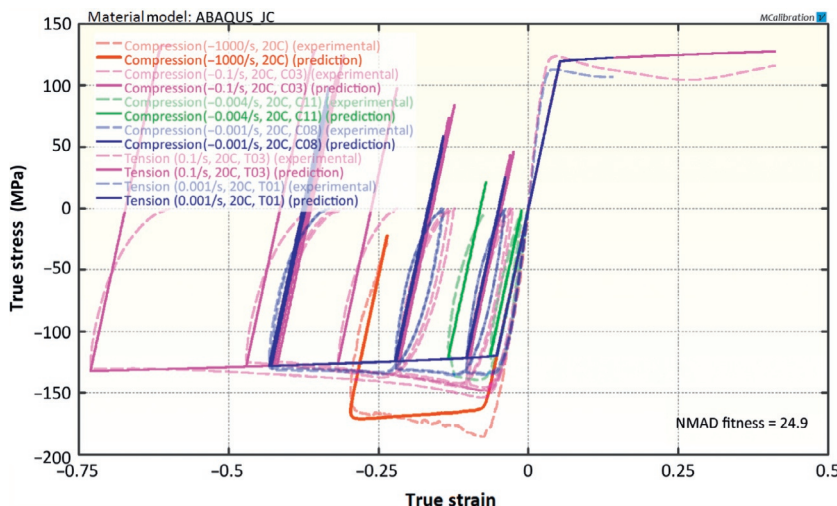


Figure 11.50 Comparison between experimental data for PEEK and the best model predictions from the JC plasticity model.

The calibrated material models for PEEK were validated by comparing small punch data (see Section 2.3.2) and indentation testing with a spherical indenter (see photo in Figure 11.54) to finite element predictions of the experimental tests.

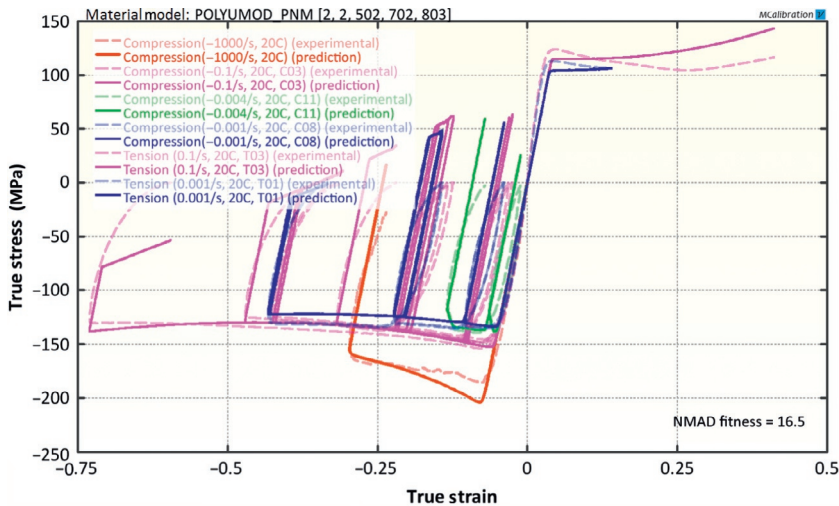


Figure 11.51 Comparison between experimental data for PEEK and the best model predictions from the PN model with two networks.

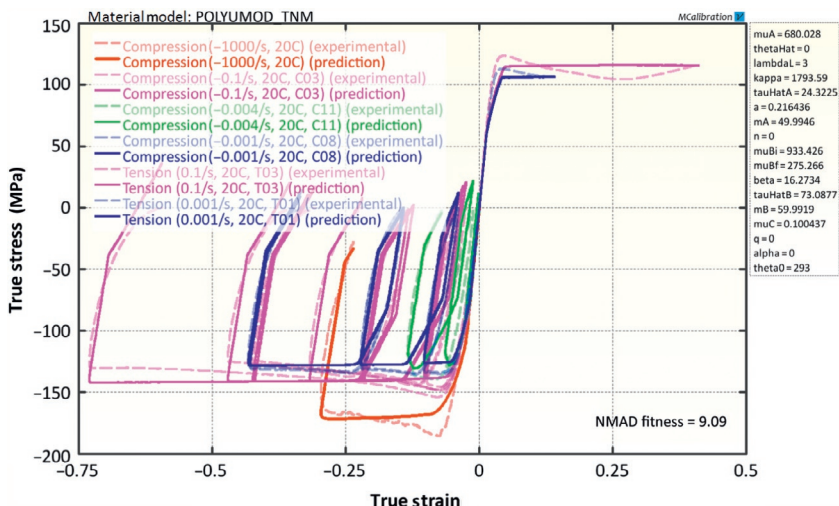


Figure 11.52 Comparison between experimental data for PEEK and the best model predictions from the TN model.

Figure 11.53 shows the force-displacement results from a small punch experiment and the corresponding results from the BB model, the TN model, and the JC model. The figure shows that the TN model is more accurate at predicting the force response of this multiaxial test than the BB and JC models. This results also

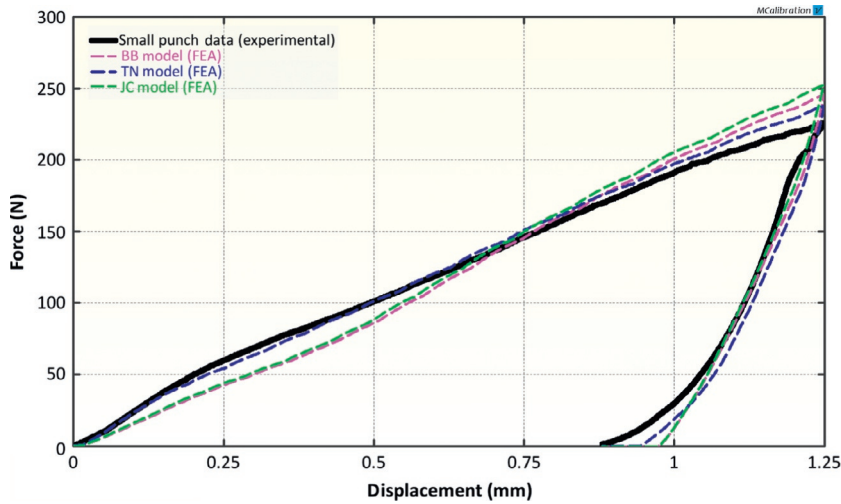


Figure 11.53 Comparison between experimental small punch data for PEEK and FE predictions from a few different material models.

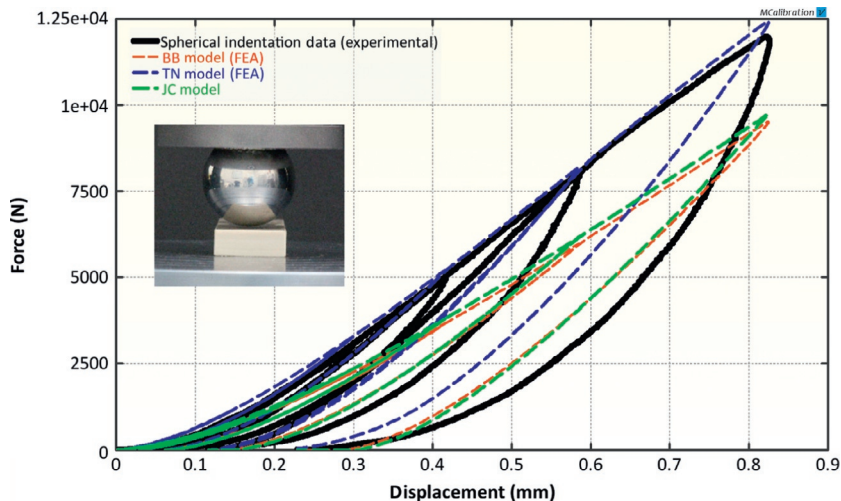


Figure 11.54 Comparison between experimental small punch data for PEEK and FE predictions from a few different material models.

demonstrates that these models can be used to accurately predict the response of a material under multiaxial loading even if they have only been calibrated using uniaxial data.

Results from the spherical indentation test and the model predictions from the BB model the TN model, and the JC model are shown in Figure 11.54. The results shown in this figure are

similar to the results from the previous figure in that the TN model is more accurate than the BB and the JC models. Again, these models can accurately predict the response of a material under multiaxial loading even if they have only been calibrated using uniaxial data.

11.10 Exercises

1. The case studies presented in this section cover a wide variety of different materials. Are there any polymeric material classes that are not included?
2. Explain why a hyperelastic material model cannot accurately represent the behavior of the ABR.
3. Explain why adding Mullins damage to the material models of the ABR increases the accuracy of the predictions?
4. What other aspects than accuracy can be important to consider when selecting a material model?
5. Why does not LVE provide an accurate representation of the experimental data for the rubber materials studied in this chapter?
6. Which hyperelastic material model would you select for the CR material? Why?
7. Explain how the stress can increase in magnitude during a stress relaxation experiment.
8. What material model would you select for the Santoprene material? Why?
9. Why is the compressive stress so much higher than the tensile stress (at the same strain level) for the PTFE material? What material model can capture the stress difference?
10. Which material models can capture a large drop in stress after yielding?
11. Why does not a plasticity model work well for PEEK?

References

- [1] J.S. Bergström, L.B. Hilbert Jr., A constitutive model for the large deformation thermomechanical behavior of fluoropolymers, *Mech. Mater.*, 37 (2005) 899-913.
- [2] R.B. Dupaix, Temperature and rate dependent finite strain behavior of poly(ethylene terephthalate) and poly(ethylene terephthalate)-glycol above the glass transition temperature, Ph.D. thesis, MIT, 2003.